Agglomeration Effects on the Drying and Dehydration Stability of Pharmaceutical Acicular Hydrate: Carbamazepine Dihydrate

ARTICLE *in* INDUSTRIAL & ENGINEERING CHEMISTRY RESEARCH · NOVEMBER 2009

Impact Factor: 2.59 · DOI: 10.1021/ie9011968

3 AUTHORS, INCLUDING:

Jiyi Khoo
GlaxoSmithKline plc.
16 PUBLICATIONS **89** CITATIONS
SEE PROFILE

Daryl Williams
Imperial College London
67 PUBLICATIONS **1,253** CITATIONS
SEE PROFILE

Agglomeration Effects on the Drying and Dehydration Stability of Pharmaceutical Acicular Hydrate: Carbamazepine Dihydrate

Ji Yi Khoo, Jerry Y. Y. Heng, and Daryl R. Williams*

Surfaces and Particle Engineering Laboratory, Department of Chemical Engineering, Imperial College London, South Kensington Campus, London SW7 2AZ, United Kingdom

The effects of agglomeration on the dehydration kinetics and stability of carbamazepine dihydrate were investigated and are reported here. The prepared dihydrate agglomerates were sieved into six particle size distributions, ranging from 75 to ~1800 μm, prior to gravimetric dehydration studies. It was concluded that when these agglomerates exceed a critical agglomerates size, they then retain an excess amount of physically adsorbed (unbound) water relative to the smaller agglomerate sizes. Specifically, agglomerates with particle diameter >1400 μm held up to 57.2 wt % of unbound water, residing within the funicular regime of moisture saturation. These larger agglomerates exhibit a distinct and densely packed particle structure, leading to a relatively more stable dihydrate, having a lower critical humidity of 20% RH (0.0039 kg_{water}/kg_{air}) at 25 °C, than those agglomerates without inclusion of unbound water. This work demonstrates that the moisture stability performance of agglomerated solids is dependent both on the intrinsic water sorption properties of the component materials as well as the local microstructure that evolves within the agglomerated solids. Furthermore, this work also demonstrates that the moisture stability of a solid state form can be strongly influenced by local particle microstructure, which thus provides another strategy for improving moisture stability of formulated products.

Introduction

Most organic crystalline forms exhibit anisotropic structural properties, leading to the formation of different crystal habits. Acicular or needle-like crystals provide special challenges in the secondary processing operations (e.g., suspension-type crystallization and granulation) in the pharmaceutical industry, due to their tendency to form cake or agglomerates with resultant inclusion of liquid solvent.[1,2] The inclusion of liquid solvent not only decreases the purity of the drug formulation, but this liquid solvent, released during the drying process, can participate in various undesirable physical and chemical material transformations.[1] Even if the drug substances are poorly soluble in the liquid solvent, the presence of any dissolved solute may facilitate the formation of crystalline bridges between the particles during the drying process.[2] Any resultant morphological transformations may have a detrimental effect on the final solid properties, including thermal and mechanical properties, which could potentially reduce the bioavailability or the storage envelope of such drug substances.

Though agglomerates of different sizes and surface chemistry are known to retain different amounts of liquid solvent and while the agglomeration mechanisms of acicular crystals have been widely studied,[1,2,4,5] the role of these trapped water molecules on the stability (physical and chemical) of the drug substances is not well understood. In this work, we have investigated the influence of physically trapped (unbound) water on the drying/dehydration kinetics and stability of an agglomerated hydrate. This study enables us to understand and elucidate the transport mechanisms of both unbound water and hydrate water (water of crystallization) prevalent during the drying process. Subsequently, this knowledge allows us to map out the stability region of agglomerated hydrates reported here as well, highlighting the effect of agglomerate structure on this stability performance.

* To whom correspondence should be addressed. Tel: +44 (0)20 7594 5611Fax: +44 (0)20 7594 5700. E-mail: d.r.williams@imperial.ac.uk.

The model compound used in this work is carbamazepine (CBZ) dihydrate. CBZ dihydrate is a widely recognized stoichiometric channel-type hydrate, with very poor solubility in water (0.4 mg/mL at 25 °C).[3] CBZ anhydrate has served as a potent anticonvulsant and mood-stabilizing drug for the last 30 years.[4] The oral absorption of the anhydrate form is slow, erratic, and unpredictable in humans, owing to its slow rate of dissolution and rapid conversion to CBZ dihydrate[5] once suspended in aqueous media or exposed to a high relative humidity (>70% RH at 22 °C).[6]

Experimental Section

Materials. Commercial CBZ anhydrate ($C_{15}H_{12}N_2O$, MW = 236.27 g/mol) was used as received (Sigma-Aldrich Ltd., Gillingham, UK). CBZ dihydrate was prepared by suspending the CBZ anhydrate powder in deionized water (0.015 g of solid/mL of water) at room temperature. The suspension was stirred at 100 rpm for 24 h to form the CBZ dihydrate. The crystals obtained were acicular shaped. The slurry was then filtered via suction, prior to air drying in a fume cupboard for 3 h. CBZ dihydrate was sieved into six particle size distributions (sieve fractions), 75−180, 180−250, 250−500, 500−710, 710−1400, and >1400 μm, using a series of ASTM standard sieves (Endecotts Ltd., London, UK). During the sieving process, the partially dried CBZ dihydrate agglomerated. All CBZ dihydrates were kept in sealed glass vials and stored at appropriate controlled humidities to maintain the sample's integrity.

Dynamic Vapor Sorption (DVS). DVS (Surface Measurement Systems Ltd., London, UK) gravimetrically measures the isothermal drying and dehydration rate of CBZ dihydrate, with a balance resolution of 0.1 μg and data saving at every 1 min. The partial pressure in the atmospheric flow DVS is regulated between 0% P/P_0 and 98% P/P_0 (±1% P/P_0) of water vapor at a constant flow rate of 200 sccm (air volumetric flow rate at standard condition).

Mercury Porosimetry Analysis (MPA). MPA was conducted with an AutoPore IV 9500 Series porosimeter (Mi-

10.1021/ie9011968 CCC: $40.75
Published on Web 11/20/2009

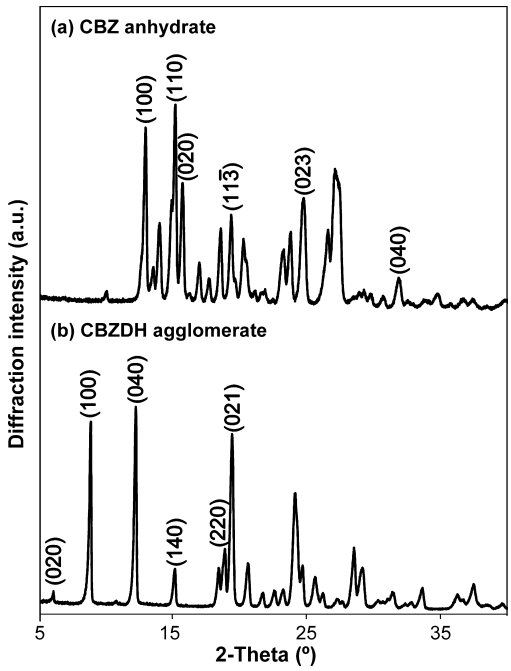

Figure 1. Powder X-ray diffraction patterns of (a) CBZ anhydrate form III and (b) CBZ dihydrate agglomerate.

cromeritic Instrument Co., Norcross, GA). The analysis was conducted at low and high pressure ranges. The pressure was incrementally increased up to 33 000 psia and 10 s was allowed to elapse before the volume of intruded mercury was recorded at each pressure. Prior to the Hg porosimetry analysis, all samples were conditioned in the DVS system under 50% RH at 25 °C for 1 day, in order to remove any excess adsorbed water.

Scanning Electron Microscopy (SEM). A TM-1000 tabletop microscope (Hitachi Ltd., Tokyo, Japan) was employed to observe morphological changes of CBZ samples. Samples were gold-coated prior to analysis. SEM micrographs, up to 2000× magnification, were taken at 15 kV beam acceleration voltage.

X-ray Powder Diffraction (XRPD). XRPD analysis was performed with an X'Pert PRO diffractometer (PANalytical, Almelo, The Netherlands) to confirm the crystallinity of the prepared CBZ dihydrate samples. Samples were scanned from 5° to 40° (2θ) using a step size of 0.016° (2θ), with nickel-filtered Cu α radiation (θ = 1.542 Å) at 40 kV and 40 mA.

Results and Discussion

Crystal Structure Identification. Powder XRD analysis (Figure 1) has confirmed that all the agglomerates formed were CBZ dihydrate (monoclinic crystal system, space group $P2_1/c$).[7] No traces of CBZ anhydrate were found above the equipment's detection limit of <5%. Post dehydration agglomerates were identified as the initial CBZ anhydrate form III (monoclinic crystal system, space group $P2_1/c$).[8]

Characterization of CBZ Dihydrate Agglomerates. Microscopic observations reveal that the agglomerates formed during the sieving process came in various macroscopic shapes, spherical and oblong. Figure 2 illustrates the surface topography of CBZ dihydrate agglomerates for two different particle size distributions, >1400 μm (Figure 2a,b) and 75−180 μm (Figure 2c,d). The densely packed >1400 μm agglomerates were in fact spheroidal in shape with larger pores occasionally observed visually on the particle surface. The shape of 75−180 μm samples, however, was mostly oblong with irregular outlines, and the agglomerate packing was characterized by a rigid and open structure.

The size of the primary particle within these agglomerates was almost identical, as the average length of the primary crystals in >1400 μm agglomerates was 13.36 ± 4.23 μm; meanwhile, the primary crystals of 75−180 μm agglomerates were 13.66 ± 4.0 μm. The primary crystals had an aspect ratio of >10 and a crystal diameter within the range of 0.8−1.8 μm. We could subsequently disregard primary crystal size as the dominant factor and therefore suggested that it is the differences in packing and pore structure of these agglomerates that influence the amount of solvent inclusion. In all agglomerate sizes, crystalline bridges that held several single acicular CBZ dihydrate crystals together were also observed.

The agglomerate pore structure was then characterized with mercury porosimetry analysis, based on the Washburn equation, which relates the intrusion pressures (ΔP) to the corresponding pore diameter, D_{pore}.

$$\Delta P = \frac{4\gamma \cos \theta}{D_{pore}} \quad (1)$$

The surface tension of mercury (γ) and contact angle between mercury and CBZ dihydrate (θ) employed in this work were 0.485 N/m and 130.0°, respectively. The Washburn analysis, however, only considers open pores, assuming they are cylindrical in shape, rather than measuring the actual internal pore size.[9]

In the porosimetry experiments reported, there are both intra- and interagglomerate contributions to the sample porosity. Here we analyzed only the porosity data, which related to the intra-agglomerate porosity using the intrusion data from 30 to 33 000 psia. Therefore, the intra-agglomerate intrusion volume (mL/g) and pore area (m^2/g) were used as comparison in this work (Table 1). There was a substantial increment by about 34% in pore volume and 93% in pore area, as the particle size distribution reached >1400 μm.

From the pore size distribution plot presented in Figure 3, it is clearly shown that only macroporosity (pore size above 50 nm) exists in the CBZ dihydrate agglomerates. Smaller agglomerates (below 1400 μm) display unimodal pore size distribution, ranging between 0.83 and 1.33 μm; however, those above 1400 μm agglomerates exhibit a bimodal distribution characteristics, having a higher number of larger pores (2.53−3.28 μm diameter). All of our CBZ dihydrate samples below 710 μm size were open-structured and were observed to be more fragile than the larger closed-packed agglomerates. Therefore, deformation of the pore structures within agglomerates might occur when the mercury intrudes, especially at the high-pressure range analysis. In addition, due to their complex and heterogeneous structures, the pore space between the acicular crystals in the agglomerate was spatially disordered; consequently, the pore size distribution values were used for comparison purpose only.

It is well-established that the densest packing of infinite straight cylinders is hexagonal, which is equivalent to the planar packing hexagonally of disks.[10] The least dense packing for the same system will result in a fully random distribution of the same straight cylinders in space. Though in our case, the cylinders are not infinite in length but have a length to diameter ratio of >10. Nevertheless, we could expect the same general observations for fiber packing to hold true.[11] It is quite clear from the SEM images shown in Figure 2 that our agglomerates adopt two quite different particle packing morphologies. In the smaller agglomerates (Figure 2d), the acicular crystals adopt a highly random orientation, while it is clear that the larger

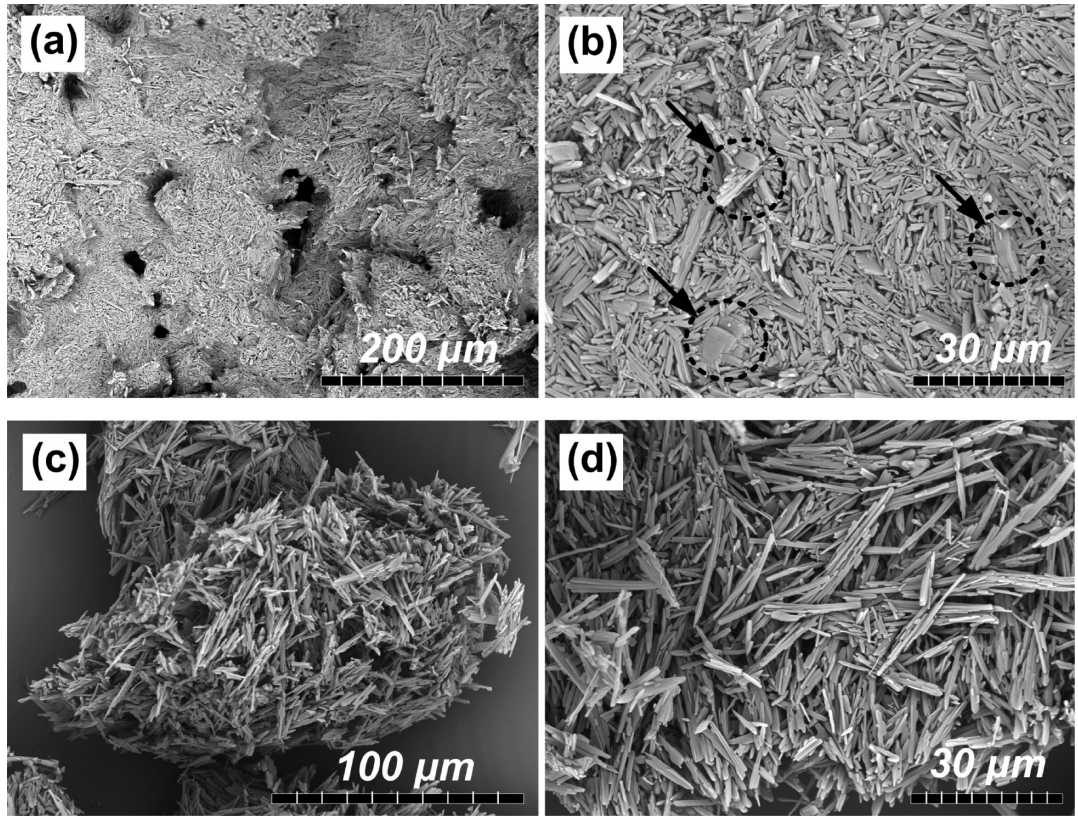

Figure 2. Surface topography of CBZ dihydrate agglomerates of different particle size: (a, b) >1400 μm and (c, d) 75−180 μm.

Table 1. Mercury Porosimetry Analysis for CBZ Dihydrate Agglomerates

agglomerate size distribution (μm)	total intra-agglomerate pore volume (mL/g)	total intra-agglomerate pore area (m^2/g)
180−250	0.783	7.049
250−500	0.815	7.032
500−710	0.822	8.465
710−1400	0.918	10.023
>1400	1.051	13.623

agglomerates adopt a much more lamellar structure, which is somewhat nematic in form (Figure 2b). Studies by Novellani et al.[12] confirm that the random 3D packing of cylindrical fibers results in a higher internal void space compared to similar 2D fiber packing. That result is intuitively sensible, though in our work we have found the converse, suggesting that either one or both our agglomerates do not exhibit fully random 2D or 3D structures. Our porosity results show a single pore size distribution for the smaller agglomerates and a bimodal pore size distribution for the larger agglomerates. The former result is consistent with a 3D random acicular particle network in the case of the smaller agglomerates. The presence of a bimodal pore size distribution in these larger agglomerates suggests that the acicular fibres in these agglomerates are not randomly distributed in either 2D or 3D. Reasons for this may relate to the water retained in these materials, as discussed later in this paper.

Dehydration Kinetics of Bound and Unbound Water. For the isothermal dehydration studies, CBZ dihydrate agglomerates 75−180, 180−250, 250−500, 500−710, 710−1400, and >1400 μm (up to about 1800 μm) in size were subjected to dry and humidified environments (0% to 80% RH, step size 10% RH), over the temperature range of 25−50 °C. The moisture content, X_A, in this work is expressed as moisture quantity per unit weight

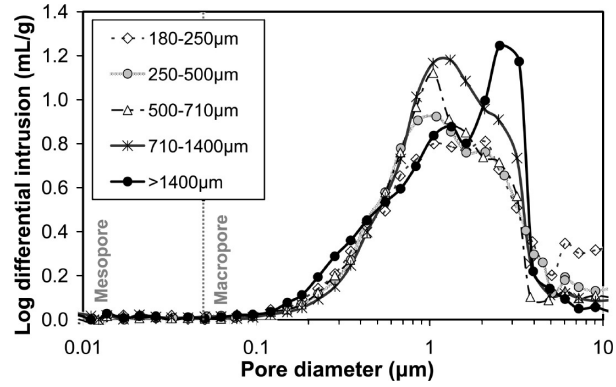

Figure 3. Pore size distribution obtained from Hg porosimetry for CBZ dihydrate agglomerates of different particle size distributions.

of the dry solid (CBZ anhydrate). For a stoichiometric CBZ dihydrate with two water molecules (MW for H_2O = 18 g/mol), the total moisture content is determined as 0.1524 (eq 2). Therefore, any moisture content values reported above 0.1524 are considered as the excess unbound water, i.e., physisorbed or condensed water.

$$X_A = \frac{\text{Mass}_{\text{Wet}} - \text{Mass}_{\text{Dry}}}{\text{Mass}_{\text{Dry}}} = \frac{\text{Mass}_{H_2O}}{\text{Mass}_{\text{CBZ}}} = \frac{2 \times 18 \text{ g/mol}}{236.269 \text{ g/mol}} = 0.1524 \quad (2)$$

From Figure 4, all agglomerates below 710 μm retained a negligible amount of unbound water, <0.02 wt % (mass of unbound water per unit mass of dry solid). On the basis of the established condensation behavior of water in soils and the saturation regime map for granules,[2,13] these agglomerates in this size distribution were well within the pendular regime, whereas for the agglomerates between 710 and 1400 μm, the

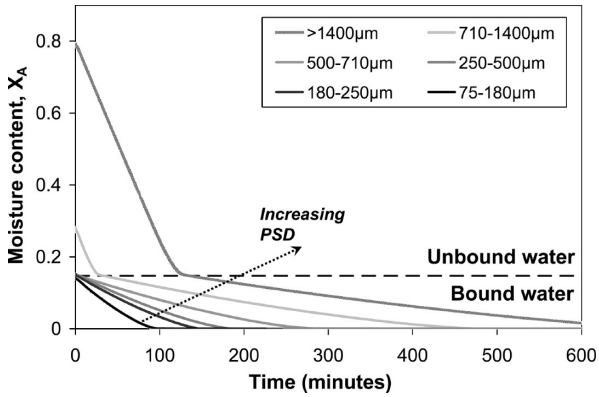

Figure 4. Dehydration profile of CBZ dihydrate agglomerates of different particle sizes at 0% RH and 30 °C.

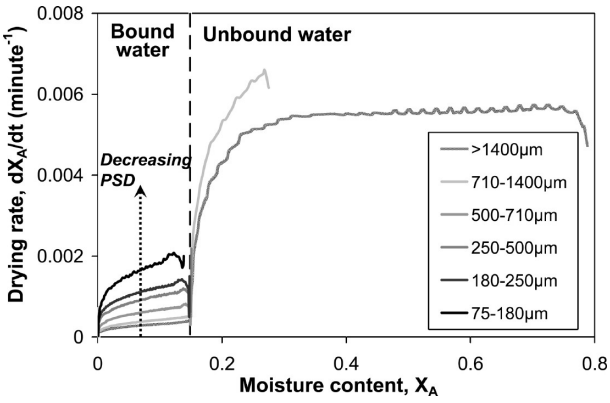

Figure 5. Krischer plot for CBZ dihydrate agglomerates of different particle sizes at zero humidity and 30 °C.

saturation state just fell within the funicular regime, with higher unbound water content of 12.1 ± 1.5% wt. Surprisingly, agglomerates >1400 μm retained a significant amount of unbound water, 57.2 ± 2.0% wt.

The smaller CBZ dihydrate agglomerates contain fewer crystals and, as expected, dehydrate faster due to higher surface area for mass ratios (Figure 4). However, as the agglomerate size goes up to 710 μm and above, the drying of unbound water and dehydration of bound water proceed via a two-step mechanism. It was demonstrated by the smooth and linear drying rate, prior to an inflection point at X_A of 0.15 for the change in gradient, which refers to the slower diffusion of bound water. This also implies that drying and dehydration processes do not occur simultaneously in those >710 μm agglomerates. This observation agrees with the work of Suraya and Suryanarayanan,[1] although their CBZ dihydrate primary particles were relatively larger (about 100 μm) and contained ~30% (by mass) of unbound water.

The drying and dehydration rates dX_A/dt (min^{-1}) were subsequently determined by computing the time derivative of the moisture content curve. Figure 5 displays two distinct stages for bound and unbound water, illustrating the three classical drying phases (i.e., induction period, constant rate, and falling rate),[14] particularly at the removal of the unbound water.

The induction period observed here is quite short and erratic. The constant rate phase, however, is clearly shown, especially for >1400 μm agglomerates. This observation is due to the constant saturation of water on the sample surface, indicating that the rate of water diffusion onto the surface is larger than the rate of water evaporation from the surface. The falling rate phase commenced when the water vapor pressure was insufficient to keep the surface saturated with water vapor, and thus, the sample started to dry out.[15] At this stage, the drying rate was governed by the internal moisture diffusion of CBZ dihydrate crystals, and the influence of external variables (i.e., heat and mass transfer coefficients) diminished.

Table 2. Activation Energies for Removal of Bound and Unbound Water in CBZ Dihydrate

agglomerate size distribution (μm)	activation energy, E_a (kJ/mol)	
	bound water	unbound water
180−250	61.4 ± 1.3	
250−500	77.0 ± 5.5	
500−710	79.9 ± 4.1	
710−1400	103.9 ± 2.4	32.3 ± 0.3
>1400	107.5 ± 1.8	35.0 ± 0.2

Activation Energy of Drying and Dehydration. Table 2 summarizes the activation energies (E_a) of drying and dehydration for CBZ dihydrate, determined from Arrhenius plots of drying/dehydration rate constant at different temperatures. Not surprisingly, the rapid dehydration rate of those smaller particles was reflected in a lower activation energy. This may be rationalized by the larger specific surface area for effective mass transfer and the shorter hydrate channel to overcome. Since unbound water is physically adsorbed on the crystal surface and behaves like pure water, the drying E_a values are similar to the enthalpy of vaporization of water, which is about 43.3 kJ/mol. The dehydration E_a values of agglomerates below 710 μm are in agreement with the reported E_a values (88[1] and 68.8 kJ/mol[16]). Nevertheless, the dehydration E_a values for agglomerates ≥710 μm are about 40% more than those smaller agglomerates that have no unbound water. This implies that the presence of unbound water increases the stability of these hydrate agglomerates.

Retention of Unbound Water in Agglomerated Dihydrate. The substantial holding capacity of unbound water in large agglomerates (particle size distribution from 1400 to ~1800 μm) could due to the "forced" hydration preparation method. The packing transition, which results in closed and dense agglomerate structure, is illustrated in Figure 6.

Since the hydration method (stage A) involves total immersion of the poorly soluble crystallized dihydrate, it is highly probable that there exists a hydrophobic interaction between the crystals.[17] This concept relates to the entropy nature of hydrophobic molecules to form agglomerates in an aqueous medium, for instance, separation of oil and water.[18] The water molecules prefer to form the stronger hydrogen-bond network, resulting in the segregation and effective mutual attraction of the hydrophobic CBZ dihydrate crystals. The significant effect of hydrophobic particle surfaces in total immersion of water was evidently shown in previous literature,[19,20] in which the hydrophobic free energy is proportional to the surface area for interaction between hydrophobic solutes and water molecules.[18] Consequently, the acicular shape of CBZ dihydrate was able to provide the high surface coverage for effective contact area between each other, thus increasing the likelihood of agglomeration, as depicted in stage B (Figure 6).

As the resultant dihydrate was being filtered via suction, there are two preparation scenarios: those particles having crystal surfaces saturated with a high amount of unbound water molecules and those with just a slight moisture excess. The former case would allow a certain degree of "surface plasticity", a term proposed by Newitt and Conway-Jones,[2] where by this excess unbound water was able to hold the primary particle by the effect of cohesion due to capillary forces (stage C). Meanwhile, in the latter case, the primary particles were just

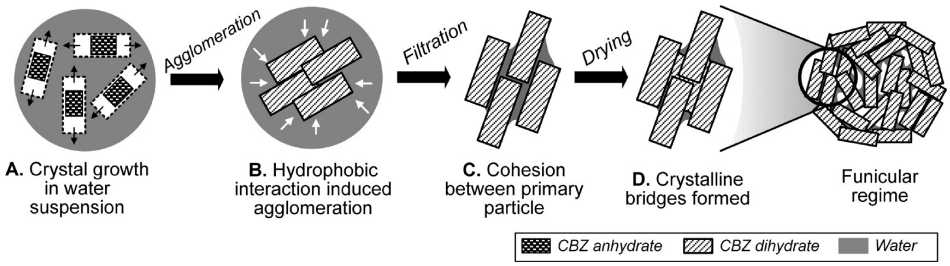

Figure 6. Proposed moisture-induced packing transition stages of agglomerated acicular CBZ dihydrate crystals of particle size from 1400 to ~1800 μm.

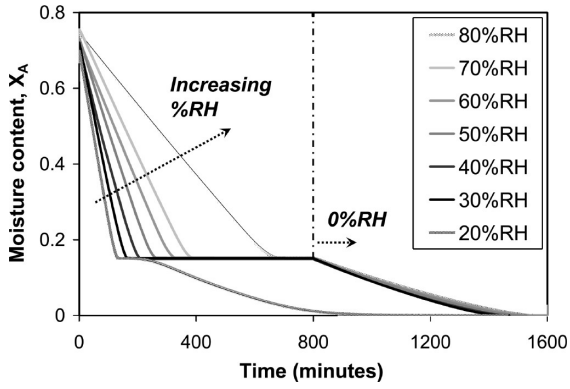

Figure 7. Dehydration profile of CBZ dihydrate agglomerates (>1400 μm) under different levels of humidity at 30 °C.

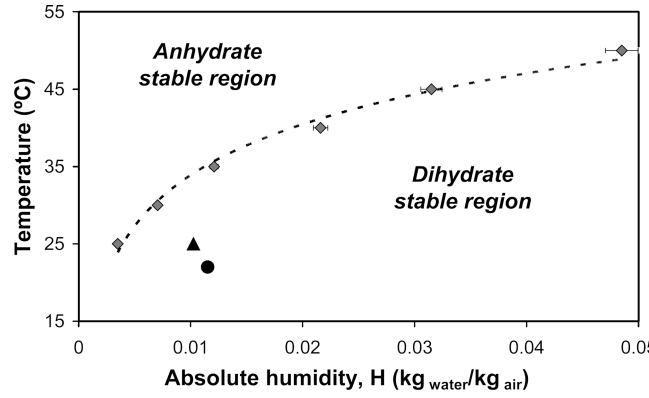

Figure 8. Critical absolute humidity values for agglomerated CBZ dihydrate (>1400 μm, funicular regime). ▲ and ● denote the H_c for loose crystal forms by Surana et al.[1] and Dugue et al.,[6] respectively.

sufficiently moist to form a "pendular bond" at the point of contact. During the predrying step, stage D, the slow evaporation of excess water at room temperature would form the crystalline bridges and therefore shape this densely packed structure, resulting in inclusion of the remaining unbound water molecules within the agglomerates.

Role of Unbound Water on the Stability of Agglomerated Dihydrate. It has been recognized that the CBZ dihydrate is stable above 52% RH (absolute humidity, H_c as 0.01024 kg_{water}/kg_{air}) at 25 °C.[1] Once the dihydrate was exposed to an environmental humidity below that critical humidity, loss of hydrate water will commence. To investigate the role of unbound water on the stability of CBZ dihydrate, agglomerates with particle size >1400 μm were subjected to drying conditions under different relative humidities and over a range of temperatures. An example conducted at 30 °C is presented in Figure 7.

CBZ dihydrate agglomerates were first exposed to a high humidity environment, for instance, at 80% RH (Figure 7). The loss of unbound water would begin and plateau out after ~11 h; no further water removal was observed, even at a longer time scale. Since 80% RH was well above the H_c of CBZ dihydrate, the humidity of the system was subsequently brought down to 0% RH at 800 min (illustrated by the dotted line) in order to instigate the dehydration of CBZ dihydrate. The amount of water removed under the 0% RH period correlates to the stoichiometric dihydrate, $X_A = 0.15$.

As the starting humidity decreases to 30% RH, only the removal of unbound water took place and all samples reached the equilibrium state where the remaining water content corresponds to X_A. However, at 20% RH, dehydration process commenced once the removal of unbound water was completed, as represented by the inflection point in Figure 7. It could thus be concluded that this agglomerated CBZ dihydrate managed to retain the dihydrate's integrity even at *lower humidity* than the previously reported 52% RH.[1]

Values of the critical humidity, H_c (kg_{water}/kg_{air}), of agglomerated CBZ dihydrate over a range of temperatures (Figure 8) were compared to the critical value of those crystal forms without inclusion of unbound water.[1,6] Absolute humidity values were calculated from eqs 3 and 4.[21]

$$\mathrm{RH} = 100 \times \frac{p}{p_s} \tag{3}$$

$$H = \frac{\mathrm{MW}_{H_2O} \times p}{\mathrm{MW}_{air}(P - p)} \tag{4}$$

Where p is the calculated partial pressure in mmHg; p_s is the corresponding vapor pressure (mmHg) at DVS temperature (dry-bulb), and P represents the atmospheric pressure at 760.0 mmHg.

This work shows clearly that in the case of the large agglomerates created here, agglomeration has not only impeded the dehydration process, but also been able to maintain the stability of the dihydrate form at low environmental moisture concentrations (e.g., 0.0039 kg_{water}/kg_{air} at 25 °C). The relationship of these two functions: absolute humidity and temperature clearly defines the boundary between the regions for dihydrate or anhydrate form stability.

Conclusions

Within the experimental range considered, we have demonstrated that agglomeration has notable influence on the drying and dehydration kinetics of CBZ dihydrate acicular crystals. As these agglomerates exceed a critical particle size, they tend to retain an excess amount of physically adsorbed water, up to a significant 57.2 wt % and exhibit closed pore structure. These large agglomerates (particle diameter from 1400 to ~1800 μm) occur within the funicular regime of moisture saturation and

are significantly more stable than those agglomerates without inclusion of unbound water, their integrity being retained even at a low critical humidity of 20% RH (0.0039 kg_{water}/kg_{air}) at 25 °C. Mercury porosimetry further confirmed that the total intra-agglomerate intrusion volume for the largest agglomerates was 34% higher than those smaller agglomerates. Nondestructive imaging techniques like X-ray microcomputed tomography (μCT) are proposed for future work in order to visualize and quantify the interior microstructure of the random acicular particle network. This current work demonstrates that in developing a drying strategy for active pharmaceutical ingredients (APIs) which are capable of forming hydrates, agglomeration effects as shown here can be potentially controlled and exploited to increase the stability of the desired hydrated products. Further studies using other hydrates with different morphology are required to confirm the generality of the conclusions reported here.

Acknowledgment

The authors gratefully acknowledge Imperial College for the provision of Overseas Research Studentship and Student Opportunity Funds award for J.Y.K.

Abbreviations

γ = surface tension (mN/m)
λ = wavelength (Å)
ρ = density (kg/m^3)
θ = contact angle (deg)
D_{pore} = pore diameter (μm)
E_a = activation energy (kJ/mol)
MW = molecular weight (kg/kmol)
ΔP = intrusion pressure (kPa)
p = partial pressure (mmHg)
p_s = vapor pressure (mmHg)
P = atmospheric pressure (mmHg)
H_c = critical absolute humidity (kg_{water}/kg_{air})
sccm = standard cubic centimeters per minute [cm^3/min (STP)]
X_A = total moisture content
dX_A/dt = dehydration rate (min^{-1})

Literature Cited

(1) Surana, R.; Pyne, A.; Suryanarayanan, R. Solid−vapor interactions: Influence of environmental conditions on the dehydration of carbamazepine dihydrate. *AAPS PharmSciTech* **2003**, *4*, 68.

(2) Newitt, D. M.; Conway-Jones, J. M. A contribution to the theory and practice of granulation. *Trans. Inst. Chem. Eng.* **1958**, *36*, 422–441.

(3) Rodriguez-Hornedo, N.; Murphy, D. Surfactant-facilitated crystallization of dihydrate carbamazepine during dissolution of anhydrous polymorph. *J. Pharm. Sci.* **2004**, *93*, 449–460.

(4) Post, R. M.; Ketter, T. A.; Uhde, T.; Ballenger, J. C. Thirty years of clinical experience with carbamazepine in the treatment of bipolar illness—Principles and practice. *CNS Drugs* **2007**, *21*, 47–71.

(5) Tayel, S. A.; Soliman, I. I.; Louis, D. Improvement of dissolution properties of carbamazepme through application of the liquisolid tablet technique. *Eur. J. Pharm. Biopharm* **2008**, *69*, 342–347.

(6) Dugue, J.; Ceolin, R.; Rouland, J. C.; Lepage, F. Polymorphism of carbamazepine: Solid-state on carbamazepine dihydrate. *Pharm. Acta Helv.* **1991**, *66*, 307–310.

(7) Harris, R. K.; Ghi, P. Y.; Puschmann, H.; Apperley, D. C.; Griesser, U. J.; Hammond, R. B.; Ma, C.; Roberts, K. J.; Pearce, G. J.; Yates, J. R.; Pickard, C. J. Structural studies of the polymorphs of carbamazepine, its dihydrate, and two solvates. *Org. Process. Res. Dev.* **2005**, *9*, 902–910.

(8) Reboul, J. P.; Cristau, B.; Soyfer, J. C. 5*H*-Dibenz[*b,f*]azepinecarboxamide-5 (carbamazepine). *Acta Crystallogr.* **1981**, *B37*, 1844–1848.

(9) Giesche, H. Mercury porosimetry: A general (practical) overview. *Part. Part. Syst. Char.* **2006**, *23*, 9–19.

(10) Bezdek, A.; Kuperberg, W. Maximum density space packing with congruent circular cylinders of infinite length. *Mathematika* **1990**, *37*, 74–80.

(11) Williams, S. R.; Philipse, A. P. Random packings of spheres and spherocylinders simulated by mechanical contraction. *Phys. Rev. E* **2003**, *67*, 051301.

(12) Novellani, M.; Santini, R.; Tadrist, L. Experimental study of the porosity of loose stacks of stiff cylindrical fibres: Influence of the aspect ratio of fibres. *Eur. Phys. J. B* **2000**, *13*, 571–578.

(13) Lu, N.; Wu, B.; Tan, C. P. Tensile strength characteristics of unsaturated sands. *J. Geotech. Geoenviron.* **2007**, *133*, 144–154.

(14) Terrier de la Chaise, B.; LePerdriel, F. The drying of granules. *Pharma Int.* **1972**, *6*, 16–22.

(15) Keey, R. B. *Drying: Principles and Practice*; Pergamon Press: New York, 1972.

(16) Han, J.; Suryanarayanan, R. Influence of environmental conditions on the kinetics and mechanism of dehydration of carbamazepine dihydrate. *Pharm. Dev. Technol.* **1998**, *3*, 587–96.

(17) Mikheev, Y. A.; Guseva, L. N.; Davydov, E. Y.; Ershov, Y. A. The hydration of hydrophobic substances. *Russ. J. Phys. Chem. A* **2007**, *81*, 1897–1913.

(18) Chandler, D. Hydrophobicity: Two faces of water. *Nature* **2002**, *417*, 491–491.

(19) Hapgood, K. P.; Farber, L.; Michaels, J. N. Agglomeration of hydrophobic powders via solid spreading nucleation. *Powder Technol.* **2009**, *188*, 248–254.

(20) Forny, L.; Pezron, I.; Saleh, K.; Guigon, P.; Komunjer, L. Storing water in powder form by self-assembling hydrophobic silica nanoparticles. *Powder Technol.* **2007**, *171*, 15–24.

(21) Moyers, C. G.; Baldwin, G. W., Psychrometry, evaporative cooling and solids drying. In *Perry's Chemical Engineers' Handbook*, 7th ed.; Perry, R. H., Green, D. W., Maloney, J. O., Eds.; McGraw-Hill: New York, 1997; pp 1−90.

Received for review July 28, 2009
Revised manuscript received October 7, 2009
Accepted October 22, 2009

IE9011968